Multi-Sensor System for Real-Time Monitoring of Laser Micro-Structuring

Milena Zuric, Oliver Nottrodt and Peter Abels

Fraunhofer Institute for Laser Technology ILT, Steinbachstr. 15, 52074 Aachen, Germany
E-mail: milena.zuric@ilt.fraunhofer.de

Constant demand for increase in efficiency of USP-laser micromachining, leading to growing pulse repetition rates and scanning speeds, makes the online process monitoring and control progressively more challenging. However, real-time process monitoring is essential in order to predict the quality of the processing result, accelerate parameter studies or discover processing errors during the machining. Fraunhofer ILT develops a multi-sensor system to meet this challenge, collecting diverse real-time data on the process and its environment with a high sampling rate and spatial resolution.

DOI: 10.2961/jlmn.2019.03.0008
Keywords: real-time monitoring, online process monitoring, FPGA based data acquisition, laser micromachining, ultrashort pulse laser structuring

1. Introduction

The emergence of reliable ultrashort-pulse laser systems has opened a big market for high-precision micromachining. Individually micro-machined components have been highly demanded in different industrial sectors, ranging from medical over electronics to automotive and aerospace industry [1].

Laser ablation of metals is, however, a complex process that needs to be developed individually for specific requirements and materials. High quality results imply the minimization of the degree of melting and the simultaneous maximization of the ablation rate. Different workpiece features such as thermal conductivity, reflectivity, melting and vaporization temperature define important boundary conditions for the adjustment of the processing parameters leading to time-consuming trial-and-error parameter studies. Additionally, internal chemical or structural irregularities as well as the surface unevenness or uncleanness of the workpiece may deteriorate the processing result. Furthermore, stochastically occurring disturbances during the processing, e.g. plasma or particle shielding, can also negatively affect the quality of the resulting structure [2].

For these reasons, online process monitoring is of great importance for the quality assurance of the ultra-short-pulse laser micromachining. Closed-loop control or feedback to the machine operator would accelerate parameter studies and increase the process stability in production. On the other hand, real-time monitoring of the USP-micromachining represents a great challenge, due to the high spatial resolutions of the resulting structures as well as the growing processing speeds: Achievable repetition rates have reached over 50 MHz and beam deflection speeds more than 10 m/s [3]. With high-speed scanning systems based on polygon scanners, speeds of even up to 1000 m/s have been realized [4]. In order to meet this challenge, Fraunhofer ILT develops a multi-sensor system for real-time high-speed process and machine condition monitoring. Simultaneous monitoring of both the process and its surroundings enables any environmental sources of errors to be identified and excluded before analyzing the machining process itself.

2. State of The Art

Process monitoring of laser-based manufacturing has been a subject of research for many decades. In case of traditional laser applications, such as laser welding, many approaches have been reported. They are based on various types of detectors, including monitoring of process emissions, i.e. acoustic, IR-, VIS-emissions as well as the back reflection of the machining laser. For example, a thorough investigation on collection of the laser back reflection by means of axially and laterally integrated photodiodes is given in [5]. An exhaustive overview of process monitoring techniques for laser welding is presented in [6]. This comprehensive review references various pre-, post- and in-situ monitoring approaches as well as sensor combinations for laser welding applications. More recent publications describe detection of high frequency airborne- as well as structure-borne acoustic emissions [7] and employment of machine learning algorithms on welding seam images collected by multiple cameras [8]. Recording of process emissions and laser back reflection, including multi-sensor system approaches have also been abundantly described for cutting [9,10], as well as for cladding and additive manufacturing [11–13].

In contrast to other laser-based processes, literature of monitoring of USP-laser micromachining is still scarce. This is not surprising, as it is a more recent technology, which brings additional challenges to real-time monitoring, i.e. much smaller structure sizes and high processing speeds. In case of USP-laser drilling, publications include detection of the breakthrough by coaxial and lateral observations of various process emissions for different drilling techniques [14,15]. Beside breakthrough, online hole depth measurement has been thoroughly investigated. Reported approaches are based on different techniques, such as self-mixing interferometry [16] and shock wave detection by

piezoelectric transducers [17]. An investigation on plasma generated by laser drilling was presented in [18] and has also shown potential for online hole depth monitoring. Multi-sensor approaches by means of simultaneous acoustic and optical sensing through laser-beam deflection probing and a video camera, have also been reported [19]. Compared to the USP-laser drilling, online result control of USP-laser ablation represents a greater challenge, due to much lower aspect ratios and the absence of a breakthrough. Nevertheless, different concepts for monitoring of the USP-laser structuring have been reported. They range from the indirect stability assurance, by observing the process emissions, to the direct monitoring of the structure depth for predicting the ablation rate and the resulting surface roughness. Here, a summary of these approaches with an analysis of their advantages and disadvantages is given.

Monitoring of acoustic emissions can enable tracking of changes in the focus position and laser power, by analyzing the signal amplitude at the pulse repetition rate, as described in [20]. However, the process investigated in this work occurred at a low pulse frequency of 1 kHz, making the detection of the acoustic signal at this pulse repetition rate and its multiples utilizing a standard microphone possible. Investigation of audible acoustic emissions has also been employed for theoretical studies of laser ablation and described in [21] and [22]. Furthermore, microphone-based process monitoring of laser micro-structuring was patented [23], however the patent has since expired.

In order to monitor laser ablation processes with higher repetition rates in a similar manner, microphones with dynamic ranges of a few hundred kHz need to be used. This can be achieved with optical microphones, as described in [24] and [25]. However, monitoring of high-frequency airborne acoustic emission has a vast disadvantage: The signal amplitude in air is greatly attenuated with increasing frequencies. Detection of acoustic signals at few hundred kHz requires the microphone to be positioned only few millimeters near the processing zone, making a machine integration impossible. Another possibility of high-frequency acoustic signal monitoring is directly on the workpiece surface, as described in [26]. In comparison to monitoring the airborne sound, this approach entails a more complex analysis due to scattering and reflection effects at material and grain boundaries. Nevertheless, the authors report a successful detection of the focus position through pattern recognition. An unsolvable disadvantage is here, however, the necessity for mounting the sensor directly on the workpiece, making it unsuitable for production environment.

Optical emission is another type of process emission that can be monitored with a relatively cost effective equipment. This approach, integrating a photodiode in the beam path, has been investigated in [27]. The authors have shown a correlation between the VIS process emission and the focus position, laser power and the amount of ablated volume. Furthermore, they assume a possible correlation between the signal waveform and the resulting surface roughness. However, an automated detection system based on these results has not been implemented yet. Moreover, this work was based on a simplified case of structuring of points and has not been transferred to a more complicated case of 2D-structuring.

Another example for recording of VIS-emissions is given in [28], with the application in labeling of silicon wafers. Simple lines were structured for varied laser power while keeping the other parameters constant. The authors propose different statistical regression models for detecting the line width based on the recorded optical emissions. However, the successful results of this investigation are restricted to the detection of simple characteristics in structured lines and their sole dependency of laser power.

The idea to monitor visible process emissions is in fact much older, even for short and ultra-short pulse laser micromachining. Earliest reports already employed optical detectors in combination with further sensors for fundamental research of pulse duration influence on resulting thermophysical effects [29].

Another monitoring approach also used for fundamental investigations is detection of the reflected laser light on the machining surface. One example is a study of change in the material reflectance during the femtosecond ablation of metals in vacuum [30]. For this, both specular and diffuse components of the reflected laser beam were collected and focused on a joulemeter by means of a hemiellipsoidal reflector placed around the probe. The authors report a significant reduction of the reflectance for increasing laser fluence. Similar investigation was performed in the air with nanosecond pulses, also showing decrease in the surface reflectivity at higher fluencies, explained by the plasma shielding effect [31].

Real-time temperature monitoring for laser-based surface treatment has inspired developments of special pyrometers [32], focusing mainly on laser cladding. Pyrometery for various laser processes has been a research topic of this group for over a decade [33,34], however with no thorough investigations in the field of USP-laser micromachining. On the other hand, pyrometery-based fundamental research of USP-laser machining has been reported. An example of this is a study on heat absorption in a sample exposed to USP-laser radiation with a pyrometer used for the detection of the specimen temperature on its rear side while focusing the laser on its front side [35].

In a special case of multi-material laser structuring, different approaches of detecting or predicting the transition to a new material have been reported. An example of a closed-loop control, presented in [36], employs a camera and a cellular neural network (CNN) for the data analysis. The task was to detect the completion of machining a predetermined form by removing the right amount of the top material. Another possibility for an online detection of a change in the ablated material is by means of the laser induced breakdown spectroscopy (LIBS). This approach has been investigated by different research groups and described in [37] and [38].

A further example of AI- and camera-based quality control was presented in [39]. The goal was to create a database of parameters and corresponding quality results in order to realize a decision support system for process developers. An automated camera-based measurement system was developed in order to accelerate the investigation of the resulting quality and more rapidly fill the database with the processing results. A somewhat similar approach, described in [40], used artificial neural networks

for finding correlations between processing parameters and the ablation depth.

An example of a direct distance measurement integrated in the beam path was shown in [41]. This method combines the UHR-SD-OCT (ultrahigh resolution spectral domain optical coherence tomography) and a galvanometer scanner. It is able to measure topographies of small surface areas (up to 300 µm x 300 µm) with an axial resolution of almost 120 nm and lateral resolution of less than 2.5 µm. It is, however, unsuitable for a real-time detection of the material roughness, as its maximum scanning rate reaches 1.4 kHz.

Another principle based on direct distance measurement for the analysis of 2D laser micro-machined structures has been described in [42]. It is based on a principle of frequency domain low coherence interferometry (FD-OCT) integrated in the beam path. The authors report a sub-µm axial accuracy at a scanning rate of 2 kHz. The lateral resolution of an online measurement is therefore low, when performed at typical scan speeds of up to 10 m/s. This method is therefore suitable for two special cases: offline surface roughness detection either before or after the structuring and online depth detection of structures with a sufficient surface area, e.g. cavities or sample structures described in [43].

Though different approaches of process monitoring in USP-laser micromachining have been reported, none of them has yet been able to predict the quality of the resulting structure reliably and without restrictions. A tradeoff is present between directly collecting 3D-topography information with low sampling rates resulting in low spatial resolution and faster but more challenging to analyze recording of process emissions. We believe that the latter approach holds a great potential when combined with appropriate analysis techniques. By monitoring diverse process emissions simultaneously, we expect to gain a higher amount of valuable information on the process. Additionally, we observe and analyze machine, laser and environment errors or drifts to ensure constant processing conditions and eliminate environmental disturbances.

3. Data Acquisition System

The developed multi-sensor system includes different detectors for machine condition and process monitoring, which are thoroughly described in section 3.1.

In order to collect and synchronize the information from different sources with various data types and data rates, a digital data acquisition system consisting of real-time capable subsystems and a personal computer featuring analysis algorithms and a human-machine interface was developed. The detailed description of the system is given in section 3.2.

3.1 Sensors

The microstructuring machine used in this contribution is a LASER L 1000 U from AgieCharmilles with two laser sources, an ns-laser LP-V2-1-100-100-100 and a ps-laser Edgewave PX100-1-GF. In the frame of this contribution, the machine was equipped with various detectors, divided into two groups: sensors for process and for machine condition monitoring.

For the former, different signals emitted during the micromachining are observed simultaneously. One sensor for each of the following emission types is employed: VIS-, IR-, acoustic emission and the laser reflection. The sensors are arranged around the f-Theta lens, monitoring the specified emissions laterally, as shown in Fig. 1.

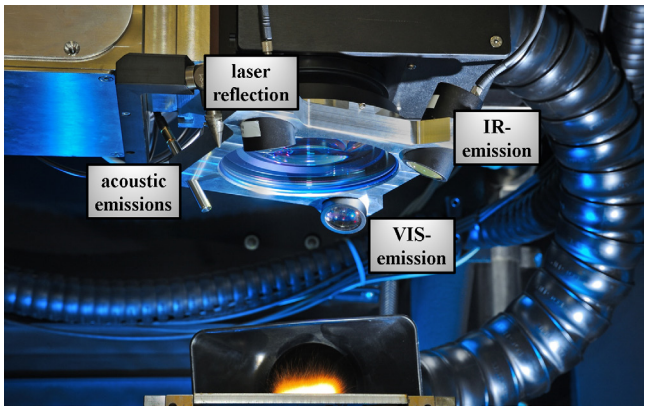

Fig. 1 Photo of the process monitoring detectors.

For the detection of the acoustic emissions, a free-field array microphone 40PH from GRAS is used. It is an airborne sound detector for audible acoustic emissions with a frequency range of 10 kHz to 20 kHz. The collection of visible process emissions occurs by a Si pin photodiode from Hamamatsu with a spectral response range of 350 nm to 1100 nm. The photodiode is protected from the laser reflection by a short pass filter with cutoff wavelength 750 nm. For the laser reflection and the infrared emissions two photodiodes of the same type are used: InGaAs pin photodiode from Hamamatsu with a spectral response range between 950 nm and 1850 nm. For detecting the laser reflection, this photodiode was installed behind a bandpass filter for the laser wavelength (1064 nm). For the detection of the IR-emission, a longpass filter with cutoff wavelength of 1100 nm is used. Each photodiode is placed behind a corresponding focusing lens. The setups ensure that the measurement spots are slightly larger than the scanning field. This way, the emissions from the whole workpiece surface are collected at all times.

Another group of sensors is employed for monitoring of the machine itself. For this purpose, the temperatures and vibrations in the following crucial points are collected: environment, machine bed, scanner and workpiece. Furthermore, a stability verification of the laser power and spot geometry is carried out using a system schematically depicted in Fig. 2.

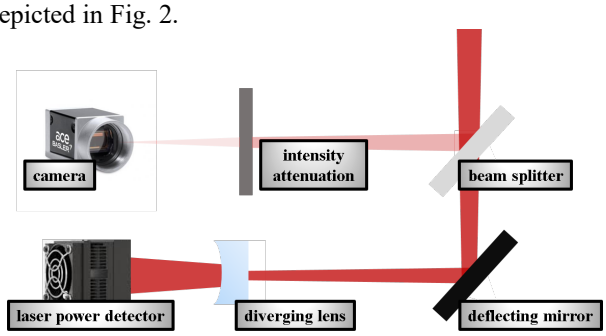

Fig. 2 Schematic depiction of hardware arrangement for laser spot geometry and power monitoring.

This system is integrated in the machine beside the workpiece mount. It comprises a UP19K-110F-H9 power detector from Gentec and a CMOS camera acA3800-10gm

from Basler. The camera has a pixel size of 1.67 µm × 1.67 µm, making it possible to sufficiently resolve the laser beam in its focus position with radius of approximately 35 µm and 45 µm for the ps- and ns-laser respectively. A beam splitter is used to deflect a small portion of the beam towards the camera and guide the rest of the beam in the direction of the power meter. Further optical elements ensure correct measurement results without damaging the detectors.

3.2 Signal Acquisition and Synchronization

For acquisition and processing of the sensor data, a system represented schematically in Fig. 3 was developed. Three different data collection and preprocessing systems are used: an FPGA (field-programmable gate array), a PLC (programmable logic controller) and a PC (personal computer). This arrangement offers a great scalability and enables a direct and easy integration of sensors with different standard hardware interfaces. It additionally allows for synchronizing data from different sources with varying sample rates and data types.

The PC represents the central unit that receives and stores the data from the both real-time subsystems and enables standardized connections to further data storage and data analysis systems. Furthermore, it allows the utilization of standard data acquisition hardware for the non-real time sensor data in the system - laser power and laser spot images.

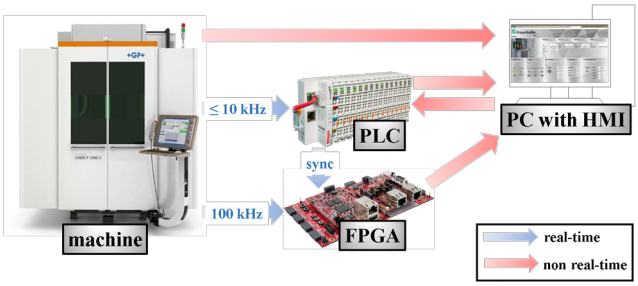

Fig. 3 Schematic depiction of the data acquisition system and its interfaces to the machine.

The spot measurement procedure is carried out before introducing changes to the machining process in terms of processing parameters, used laser, structure geometry and workpiece. This is controlled by the machine operator by accordingly programming the machine cycle. The beginning of this procedure is automatically detected by the PLC through analyzing the machine axes movement toward the measurement hardware. The PLC triggers the PC application responsible for the camera and power meter data acquisition and analysis. Fig. 4 summarizes the spot measurement routine.

As soon as the images of the laser beam are acquired, the PC application begins their analysis. The spot size and position are extracted, timestamped and saved to the hard drive and forwarded to the PLC together with the simultaneously measured laser power from the power detector. The analysis routine is normally finished by the time new laser processing starts. However, since the analysis occurs on a non-real time system, the PLC ensures the spot measurement values are not assigned to the new process monitoring data until new measurement results are received.

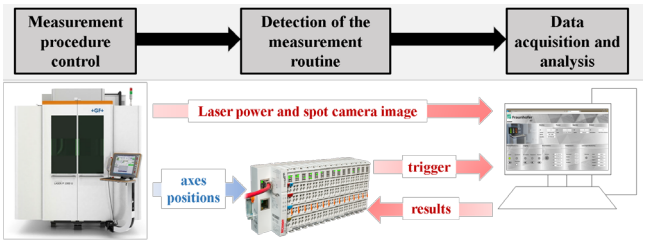

Fig. 4 Laser spot monitoring measurement procedure.

The PLC from Beckhoff has a direct access to the machine control. Beside the axis positions, it can extract information such as the beginning and end of a new processing layer. Furthermore, through the corresponding PLC terminals, temperature and vibrations signals are sampled in real time with 1 Hz and 10 kHz, respectively. The PLC features a web-based human machine interface enabling the user to monitor the measurements and control the data logging. All the communication between the PLC and the PC is carried out by the means of the ADS protocol.

For the acquisition of the high speed signals, a commercially available SoC (System-on-a-Chip) board from Xilinx is used: the MicroZed Evaluation Board with the MicroZed FMC Carrier Card. The collection of the analog data is carried out over PmodAD1 A/D converters from Digilent connected to the corresponding interfaces on the carrier card. In this manner the data from the four process monitoring sensors are sampled at a rate of 100 kHz with 12 bit resolution. The communication between the SCANLAB scanner and its control, RTC5, is guided through the FPGA board over PMOD (Peripheral Module) based interfaces. This way, the FPGA has direct real-time access to raw position data sent to the galvanometers from the scanner controller. In order to correctly map the sensor information to the positions on the workpiece surface, an optical system dependent back coordinate transformation must be taken into account. The polynomials for correcting the XY-coordinates were determined experimentally and the correction is done in the PC. The synchronization of the FPGA with the other subsystems is achieved through a modulated digital signal from the PLC. For the optimal synchronization with the scanner, the 100 kHz clock in the FPGA is directly derived from the scanner control signal. The procedure of the process monitoring data collection is shown in Fig. 5.

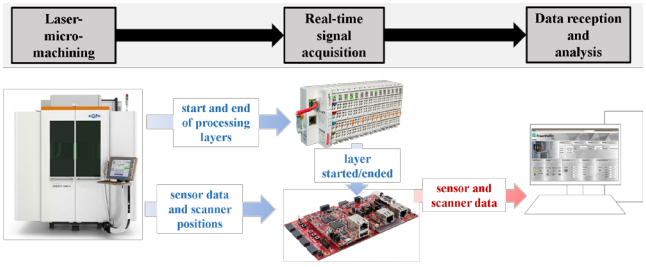

Fig. 5 Schematic depiction of the process monitoring system and procedure.

The beginning and the end of a machining layer are detected by the PLC and the information is forwarded through digital output terminals to the MicroZed over PMOD interfaces on the carrier card. Synchronously to this

information, the FPGA part of the MicroZed SoC receives the sensor data, laser modulation and scanner positions. This data is therefore recorded in real time, completely synchronously with each other at a rate of 100 kHz. The FPGA provides the data with timestamps and saves it in the RAM memory present on the board. From this point onwards, the data processing occurs in non-real-time. The processor part of the SoC takes over the Ethernet communication with the PC through which it forwards the data from the RAM. The PC application controlling the data reception organizes the data layerwise in hdf5 containers. Beside the process monitoring data from the MicroZed, these containers receive further information extracted from the PLC: axes positions, machine condition- and spot monitoring results, as well as the information input from the user in the HMI.

4. System Examination Methods

In this section, the evaluation methodology of the data acquisition system is described. A brief description of experiments that have been carried out is given in section 4.1. A qualitative analysis of the recorded data is presented in section 4.2 and 4.3 for machine condition and process monitoring, respectively.

4.1 Experiments Description

For the system evaluation, two separate series of experiments were carried out: one for machine condition and one for process monitoring.

For the former, the data was collected on a practically oriented process development case, were three different complex geometry shapes were structured on 1.2738 tool steel (40CrMnNiMo8-6-4). The average laser power was held constant and the processing type was varied between ns-laser, ps-laser and combined structuring. The temperatures and vibrations were recorded continuously to ensure that these conditions remain constant. Furthermore, the laser spot geometry and power were measured after every change of the laser and structure type, immediately before starting a new structure.

For the latter, specially designed microstructuring experiments were carried out using the same workpiece type as in the former experiments. Here, only the ps-laser was used and the structured geometries were held simple: equally spaced cavities with dimensions 4 mm by 4 mm were machined with constant number of 50 layers. The scanning occurred in an alternating manner in X- and Y-direction with a constant speed of 4 m/s. In order to assure a constant position relative to the process monitoring sensors, the position of the cavities was controlled by the machine axes movement, so that their center always remained at the center of the scanning field. At the same time, the Z-axis position was held constant, i.e. the focus position was not readjusted during the machining. Each cavity was structured with a different laser fluence, by varying the average laser power linearly between its minimum and maximum in 28 steps. Other parameters were held constant. The whole experiment was repeated for different amount of pulses per burst, between 1 and 8. All variations were additionally done for two different pulse overlaps, by switching the repetition rates between 250 kHz and 900 kHz, yielding a total amount of 448 structured cavities.

4.2 Machine Condition Monitoring

During the machining, temperatures and vibrations were logged to be analyzed and checked for abnormalities in order to exclude any fluctuations of the process influenced by its environment. This way, constant conditions for the processing were ensured at all time.

The laser spot monitoring was performed periodically at every change of the laser and the structured geometry. The analysis of the acquired images of the laser spot was integrated in the measurement cycle. The analysis procedure is graphically explained in Fig. 6.

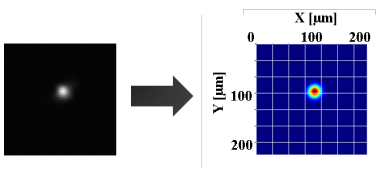

	position [µm]	FW @ 1/e² [µm]
X [µm]	118	36.2
Y [µm]	95.2	35.2

Fig. 6 Depiction of the laser spot geometry analysis.

For the spot geometry analysis, the 2D-Gaussian function is firstly fitted to the grayscale image of the laser spot. In Fig. 6 this is illustrated by the color map image. The spot radius in both X- and Y-direction as well as the position of the center point are subsequently extracted. In order to filter out any fluctuations that can originate from the machine or measurement equipment, the process is done on ten sequentially acquired images. The average parameters are timestamped, saved and assigned to the rest of the monitoring data.

4.3 Process Monitoring

The fully synchronized acquisition of the scanner position and the sensor data allows for the exact assignment of the process emissions to the corresponding machining position. The sensor data can therefore be visualized in a 2D plane and qualitatively compared to an offline topography measurement, as shown in Fig. 7.

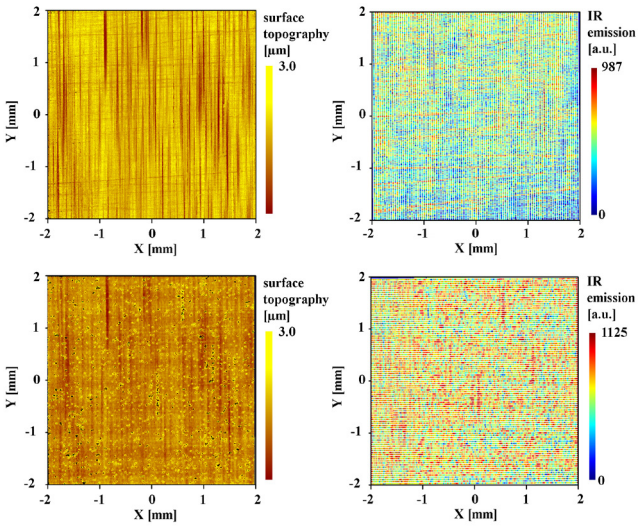

Fig. 7 Comparison of topography and IR-emission measurement before and after structuring of 50 layers. Top: surface before structuring and the IR-emission of the first layer; Bottom: surface after structuring and IR-emission of the last layer.

The four images show color map plots of surface topographies (left) and the corresponding 2D-maps of the IR-emissions (right). The topography measurement originate from a 3D optical surface profiler NewView 7300 from Zygo. The depicted measurements were performed before and after structuring and are shown in the image above and below, respectively. For the IR-emission plots, shown on the right hand side, the average intensities at each coordinate pair were taken. The upper plot shows the IR-emissions recorded while structuring the first layer, whereas the lower plot originates from the signals of the last structured layer.

Both color maps of the IR-emission show remarkable similarity to the topography images acquired offline using the surface profiler: The horizontal grooves of the surface before structuring can be recognized in the IR-emission images as areas with high average amplitude depicted in red. The vertical irregularities are on the other hand visible as areas with lower average amplitudes of the recorded signal and are represented in blue. Similar observation emerges for the graphs of the structured surfaces. Here, different point-shaped surface irregularities emerged during processing are visible as red areas in the IR-emission image. Particularly the top-right quadrant of the IR-emission image shows three larger red areas that can be assigned to the clusters of holes or CLP (cone like protrusion structures) visible in the topography image. This leads to a conclusion that a detection of the surface roughness and the presence of the CLPs by observing the IR- process emission is plausible. Both other optical emissions, the laser reflection and the VIS-emission, show similar behavior. This is expected, as the light scattering is influenced by the surface roughness, i.e. a rougher surface causes a more diffuse light reflection. On the other hand, a two-dimensional plot of acoustic emissions shows no similarity to the surface topography. This is also expected, as the raw acoustic signals predominantly include the environmental sounds. Therefore, the analysis needs to be conducted on frequencies characteristic for the process itself.

The synchronous acquisition of the laser modulation signal additionally makes the separated extraction of the data of lines along the scanning axis easier. Fig. 8 graphically explains these ratios.

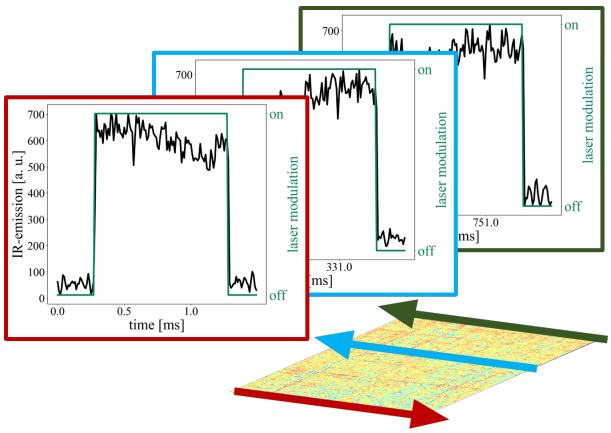

Fig. 8 Schematic depiction of the relation of the raw data and the 2D-layer representation: exemplary graphs of raw IR-emission data in the direction of scanning.

Each graph of the raw signal data originates from the recordings belonging to one scanned line. The scanning occurred in alternating directions.

For the statistical analysis of the data, given in section 5.2, only the signal waveforms within the time the laser signal was on were considered. Different waveform characteristics were extracted per scanned line, per layer and per structure. Due to the constant scanning speed and structure geometries, one layer consists of 500 lines. One structure equals one parameter variation and consists of 50 layers.

5. Results and Discussion

In this section, the first results of the data collection system are presented and discussed. Once more, they are divided into two subsections for machine condition and for process monitoring results.

5.1 Machine Condition Monitoring

Fig. 9 shows the laser spot characteristics extracted from the measurements for one complete microstructuring experiment according to the detailed description given in section 4.1.

In this experiment, two lasers were used and switched between in an alternating manner. For the clarity, the two lasers are represented in different colors with two shades indicating the X- and Y-position. The measurements are depicted chronologically. Depending on the structure geometry, they lie between 10 and 30 minutes apart. For each of the measurements an average value and standard deviation resulting from 10 sequential measurements are shown.

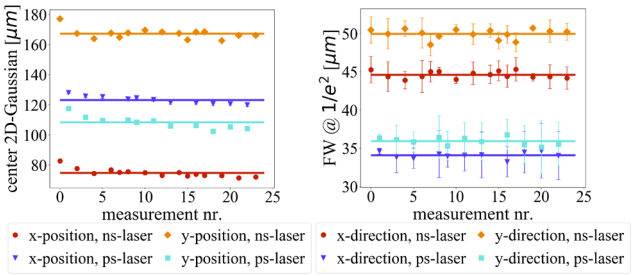

Fig. 9 Example of the beam measurement.

The distortions of the center positions are in the range of less than 10 µm for both lasers. The exact origin of this behavior needs yet to be investigated. Possible causes are the beam pointing instability in the laser, but also in other components in the beam path, i.e. scanner. Due to the measurement method, an additional influence of the machine axis kinematics cannot be excluded. A further argument supporting this claim is the low standard deviation of the sequential measurements between which no axis movement occurred. The laser spot size, however, shows stronger relative deviation in sequential measurements, which in some cases reaches over 5 µm. The cause for these deviations lies in an interplay between the machine axis inaccuracies, pointing stability of the lasers and the measurement system.

Though the presented experiments did not show any significant trend or drift of the spot position and size, the system can be employed to ensure this behavior in the long

run. By tracking these parameters during the processing, any errors resulting from the laser, mirrors, scanner and machine axes causing fluctuations in the linear component of the beam pointing can be traced back. The parallelly acquired laser power from the power meter is analyzed analogously to the spot geometry. Similarly to the spot size and position, the power measurement results showed no unusual deviations or drifts, which is why no separate graphs are explicitly shown at this point.

5.2 Process Monitoring

The following figures show analysis results of the real-time data collected in experiments described in sections 4.1 and 4.3.

Fig. 10-13 show average or maximum process emission values of the raw data of one structured layer. These characteristics are depicted for each of the 50 layers and for different amounts of pulses per burst (ppb). The figures compare the data collected at two repetition rates, 250 kHz (left) and 900 kHz (right).

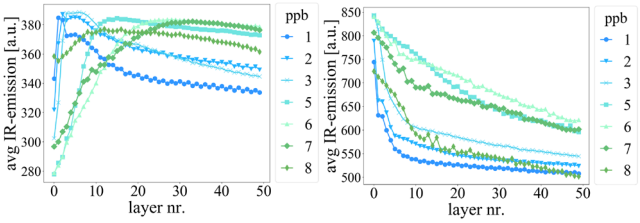

Fig. 10 Average IR-emission for each structured layer:
Left: f_{REP}=250 kHz, P_{AVG}=0.8 W, Q_P=3.14 µJ.
Right: f_{REP}=900 kHz, P_{AVG}=2.75 W, Q_P=3.0 µJ.

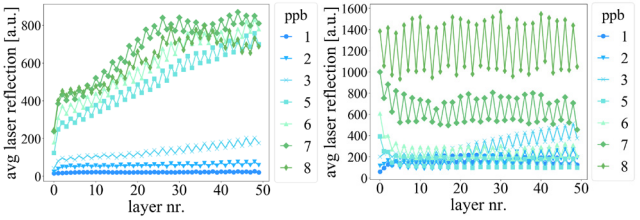

Fig. 11 Average laser reflection for each layer:
Left: f_{REP}=250 kHz, P_{AVG}=4.44 W, Q_P=17.61 µJ.
Right: f_{REP}=900 kHz, P_{AVG}=15.85 W, Q_P=17.45 µJ.

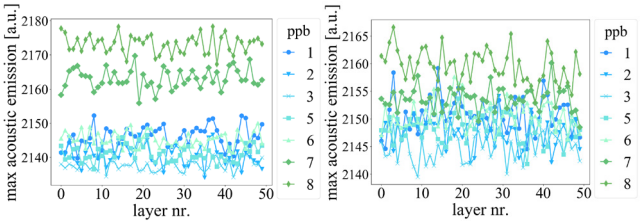

Fig. 12 Maximum acoustic emission for each layer:
Left: f_{REP}=250 kHz, P_{AVG}=8.8 W, Q_P=34.6 µJ.
Right: f_{REP}=900 kHz, P_{AVG}=31.99 W, Q_P=34.93 µJ.

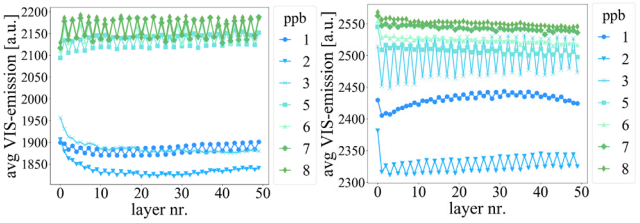

Fig. 13 Average VIS-emission for each structured layer:
Left: f_{REP}=250 kHz, P_{AVG}=16.6 W, Q_P=66.6 µJ.
Right: f_{REP}=900 kHz, P_{AVG}=58.6 W, Q_P=65.1 µJ.

The plots at different frequencies are here directly compared to the corresponding data with the most similar pulse energy. For each process emission, examples taken from different of in total 28 varied laser powers are shown.

The alternating average amplitudes originate from the alternating scanning directions and different relative distance to the sensor. The signal characteristics all show different behavior regarding the order of the structured layer. For both pulse frequencies, the IR-emissions fluctuate significantly for the first structured layers, whereas they take a more evened course from around the fifth structured layer. An additional factor influencing the signal characteristics is the defocusing, since the z-axis position was held constant during the machining.

While correlations to the order of the structured layer seem to exist, they are also different for different repetition rates and number of pulses in one burst. A similar conclusion can be drawn for the characteristics of the laser reflection and VIS-emission: The experiments revealed rather complicated dependencies of the recorded signals on the varied parameters, repetition rate and burst size, as well as the layer sequence. Additionally, these signals are not solely dependent on the varied parameters. Furthermore, the values of both optical and acoustic emissions almost constantly, but not necessarily, grow for growing number of pulses per burst. The higher IR-emission intensities are expected, due to the growing heat accumulation for the growing burst size [44]. The same explanation applies for the higher recorded thermal emissions at the higher repetition rate [45]. The growing intensity of the VIS-emissions for the growing number of pulses in one burst also correlates with the results of previous investigations [46]. The increasing amplitude of the recorded laser reflection with the increase in number of pulses in a burst can be explained by the emission signal being an integration of the reflections of more pulses. Same explanation applies to the increase in amplitude of the laser reflection with the increasing repetition rate. For the acoustic emissions, however, it has yet to be investigated if this is influenced by the process itself or by the machine. Fourier analysis has not shown any characteristic frequencies belonging solely to the process yet.

For a complete overview over the entire range of the varied parameters, average values calculated from the data in previous figures are depicted in Fig. 14-17. This representation allows for analyzing the signal dependencies on the varied laser power. Again, the data is depicted for all the varied burst sizes and a comparison is given between the two repetition rates: 250 kHz (left) and 900 kHz (right).

In general, correlations between the amplitudes of all process emissions and the varied laser power are given. While the three types of optical emissions show strong dependency on the used laser power, the acoustic emissions show a rather low rise in amplitude with the rising laser power. This is expected, since the recorded acoustic signal contains additional noises from the environment. Simple maximum amplitudes are not sufficient for describing the change in the process itself. Further analysis is needed to extract the information from this signal belonging only to the process. Correspondingly to Fig. 10-13, all the emissions show dependency on the burst size. The increasing amplitude of the process emissions for the increasing laser power is apparent and expected. The decrease in the

amplitude of the IR-emission with the increase in laser power is at first glance opposite to the expectation. The exact reason for this behavior is still to be examined. Possible explanations include the influence of different external effects on the measurement, other that the preset process parameters. A comparison of Fig. 14 and 17 reveals that the rapid drop of the IR-emission intensities for both repetition rates occurs simultaneously to the rapid rise of VIS-emissions amplitudes. Similar observation applies for the laser reflection: For the linearly increased laser power, the back reflection increases rather slowly in the areas of the rapid VIS-emission growth. This behavior correlates to the existing investigations and is explained by different effects that emerge at the increasing laser fluence [30,31]. On one hand, the laser induced surface structures can cause the diffuse reflection to outweigh the specular one [30] which would lead to less light reflected towards the sensor. Another possible cause is the plasma shielding effect [31]. In order to identify the exact explanation for this behavior in the described process, further investigations are needed.

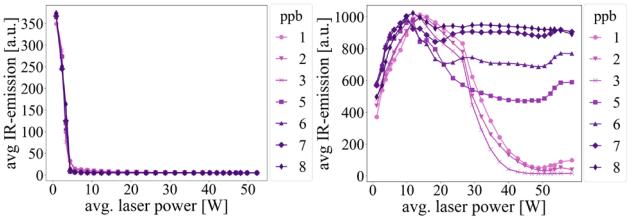

Fig. 14 Average amplitude of the IR-emissions over the varied laser power at constant f_{REP} of 250 kHz (left) and 900 kHz (right).

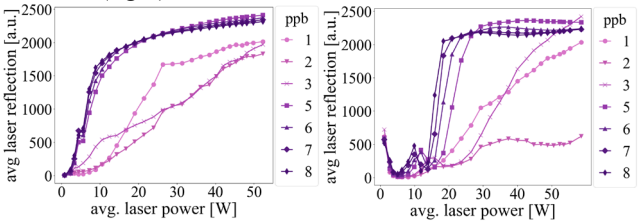

Fig. 15 Average amplitude of the laser reflections over the varied laser power at constant f_{REP} of 250 kHz (left) and 900 kHz (right).

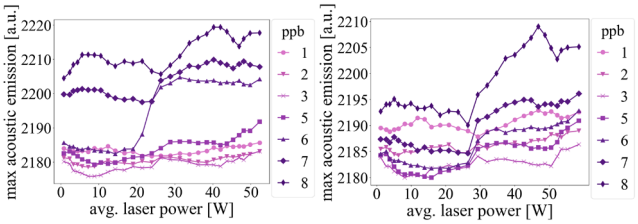

Fig. 16 Maximum amplitude of the acoustic emissions over the varied laser power at constant f_{REP} of 250 kHz (left) and 900 kHz (right).

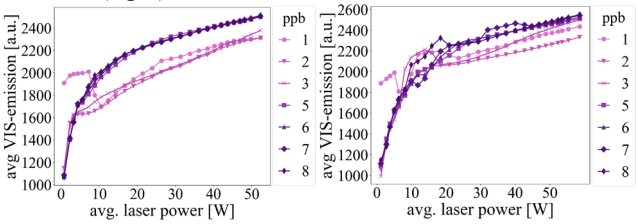

Fig. 17 Average amplitude of the VIS- emissions over the varied laser power at constant f_{REP} of 250 kHz (left) and 900 kHz (right).

Though the previous figures show interdependences between each of the emissions from the process zone and the processing parameters, the correlations are quite complex to characterize. In addition to the signals dependency on the varying processing parameters, an interplay of different physical effects plays a role on the measurement results. Complex analysis methods that take all these effects into account are needed to adequately analyze the data. Especially for predicting the quality of the result, the analysis must take into account the varying signal characteristics regarding the processing parameters.

To conclusively support this claim, signal characteristics decoupled from the amplitude influenced by the structuring parameters were inspected. Fig. 18 shows the relative standard deviation of each of the emission signals over the measured resulting surface roughness. The surface roughness measurements depicted on the X-axis originate from offline measurements using a laser scanning microscope VK 9700 from Keyence. The depicted data represent relative standard deviations of averaged process emissions at each coordinate pair in one layer. They were extracted for every last layer of the respective structure. This way, the data from the following graphs correspond the color map depiction from Fig. 7.

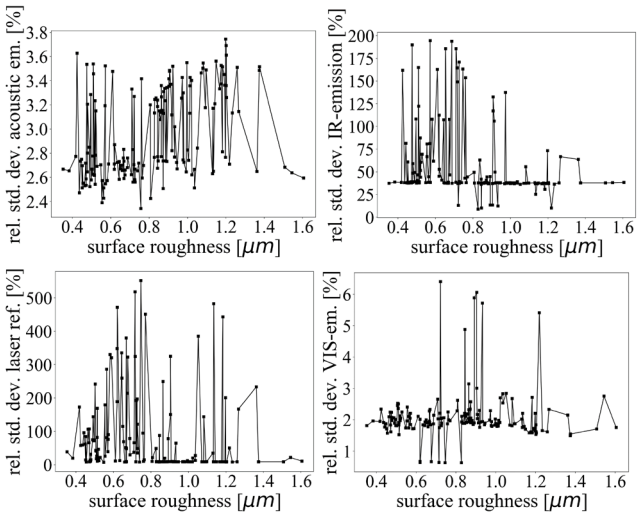

Fig. 18 Relative standard deviations of the last layer emissions over the resulting surface roughness.

Contrary to the assumption made based on the 2D data depiction, no dependency between the relative standard deviations of recorded process emissions and the surface texture is given. Until now, no correlation between the surface roughness and process emissions could be derived.

6. Conclusion and Outlook

In this contribution, a system for real-time process- and machine condition monitoring of laser micromachining is presented. The challenge solved is the acquisition, synchronization, analysis and adequate storing of the varying data types from different sources collecting information all around the process and its environment. Depending on the needed physical signal interfaces, sample rates and data types, different signal preprocessing systems are employed and the timestamped data is merged together for a centralized analysis. The most challenging part of the

data collection is the process monitoring subsystem that records and stores various process emissions completely synchronously to the machining position and laser modulation with a high sample rate of 100 kHz.

The system was validated in experiments and the first results are presented. The machine stability monitoring adequately supports the process result quality monitoring. The preliminary results of the latter show great potential for determining diverse information on the process. Correlations between the process parameters and the recorded process emissions were presented and analyzed. These need to be filtered out in order to derive quality information from the collected signals. However, this has proven to be a no easy task. Additionally, process parameters are not the only characteristics that influence the recorded signals, as complex physical phenomena and interferences affect the emergence and propagation of process emissions. The collected data dependences on the resulting surface roughness were furthermore investigated and indications of possible surface roughness detection were found. However, further investigations are needed to fully examine the complex correlations between the differing processing conditions and the recorded signals and develop a fully automated system for quality monitoring of the laser micromachining.

The system was evaluated for a simplified case of structured cavities. Nevertheless, machining of more complex 2.5D structures, exemplary shown in Fig. 19, can be monitored with the same system with no additional effort on the data acquisition side. However, these structures might yield more complex data analyses.

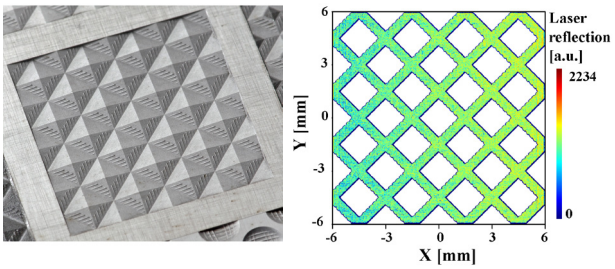

Fig. 19 Left: a 2.5D structure Right: corresponding VIS-emission of one structured layer.

Beside USP-laser micro structuring, the data collection and synchronization approach presented in this contribution is transferrable to other laser- and scanner-based applications. The flexibility of the data acquisition system allows for integration additional detectors, e.g. profilers for beam pointing monitoring. Depending on the objectives of the monitoring, new machines and applications yield adapted or newly developed analysis techniques.

Acknowledgment

Part of this project has been funded by the Fraunhofer-Society and the Federal State of North Rhine-Westphalia as a part of the High-Performance Center “Networked, Adaptive Production”.

References

[1] K. Sugioka: Nanophotonics, 6, (2017) 2913.
[2] W. Wiesemann: "Laser Physics and Applications", ed. by R. Poprawe, H. Weber and G. Herziger (Springer, Berlin, Heidelberg, New York, 2004) p.243.
[3] B. Neuenschwander, B. Jaeggi, M. Schmid, and G. Hennig: Phys. Procedia, 56, (2014) 1047.
[4] J. Schille, L. Schneider, A. Streek, S. Kloetzer, and U. Loeschner: Opt. Eng., 55, (2016) 96109.
[5] M. G. Müller: "Prozessüberwachung beim Laserstrahlschweißen durch Auswertung der reflektierten Leistung", (Herbert Utz, Munich, 2002).
[6] M. Kogel-Hollacher and T. Nicolay: Stuttgarter Lasertage, (2005) 173.
[7] M. Bastuck, H.-G. Herrmann, B. Wolter, D. Böttger, and P.-C. Zinn: WCNDT, (2016).
[8] C. Knaak, U. Thombansen, P. Abels, and M. Kröger: Procedia CIRP, 74, (2018) 623.
[9] D. Schindhelm: "In-Prozess Qualitätssicherung für das Laserstrahlschneiden von Metallen", (Herbert Utz, Munich, 2014).
[10] J. de Keuster, J. R. Duflou, and J.-P. Kruth: Int. J. Adv. Manuf. Technol., 35, (2007) 115.
[11] Angel L. Ortiz and John L. Schneiter: U. S. Patent 5045669 (1991).
[12] Y. ‐ M. Lai and N. ‐ H. Cheung: Rev. Sci. Instrum., 64, (1993) 1606.
[13] T. Purtonen, A. Kalliosaari, and A. Salminen: Phys. Procedia, 56, (2014) 1218.
[14] M. Honer: "Prozesssicherungsmassnahmen beim Bohren metallischer Werkstoffe mittels Laserstrahlung", (Herbert Utz, Munich, 2004).
[15] D. Walter: "Online-Qualitätssicherung beim Bohren mittels ultrakurz gepulster Laserstrahlung", (Herbert Utz, Munich, 2010).
[16] F. Mezzapesa, A. Ancona, T. Sibillano, and F. de Lucia: Opt. Lett., 36, (2011) 822.
[17] M. Stafe, C. Negutu, and I. M. Popescu: Shock Waves, 14, (2005) 123.
[18] J. Shin and J. Mazumder: J. Laser Appl., 28, (2016) 22008.
[19] R. Petkovšek, A. Babnik, J. Diaci, and J. Možina: Appl. Phys. A, 93, (2008) 141.
[20] P. Weber: "Steigerung der Prozesswiederholbarkeit mittels Analyse akustischer Emissionen bei der Mikrolaserablation mit UV-Pikosekundenlasern", (PhD Thesis, KIT, Karlsruhe, 2014).
[21] H. Chae and S. M. Park: Rev. Sci. Instrum., 68, (1997) 4627.
[22] S. Conesa, S. Palanco, and J. J. Laserna: Spectrochim. Acta B, 59, (2004) 1395.
[23] E. M. Bach, M. Schmidt, R. Klausecker, G. Esser, A. Otto: European Patent 1407851 (2008).
[24] F. Mitsugi, T. Ikegami, T. Nakamiya, and Y. Sonoda: Jpn. J. Appl. Phys., 51, (2012) 01AC10.
[25] F. Mitsugi, T. Ikegami, T. Nakamiya, and Y. Sonoda: Thin Solid Films, 547, (2013) 81.
[26] E. V. Bordatchev and S. K. Nikumb: Appl. Surf. Sci., 253, (2006) 1122.
[27] C. Gehrke: "Überwachung der Struktureigenschaften beim Oberflächenstrukturieren mit ultrakurzen Laserpulsen", (Herbert Utz, Munich, 2013).

[28] Y. W. Park and S. Rhee: Opt. Laser Technol., 39, (2007) 1461.
[29] P. P. Pronko, S. K. Dutta, D. Du, and R. K. Singh: J. Appl. Phys., 78, (1995) 6233.
[30] A. Y. Vorobyev and Chunlei Guo: J. Appl. Phys., 110, (2011) 43102.
[31] O. Benavides, L. de la Cruz May, and A. Flores Gil: PIERS Proceedings, (2013) 1468.
[32] M. Doubenskaia, P. Bertrand, and I. Smurov: Surf. Coat. Technol., 201, (2006) 1955.
[33] I. Smuriv, V. Martino, M. Ignatiev, and G. Flamant: J. Phys. IV France, 04, (1994) 147.
[34] I. Smurov and M. Doubenskaia: Proc. SPIE, 7356, (2009) 73560T-1.
[35] E. Principi, R. Cucini, A. Filipponi, A. Gessini, F. Bencivenga, F. D'Amico, A. Di Cicco, and C. Masciovecchio: Phys. Rev. Lett., 109, (2012) 25005.
[36] P. Strohm, O. Krause, A. Blug, D. Carl, M. Panzner, and H. Höfler: SENSOR+TEST Conferences, (2011) 60.
[37] R. Kunze, G. Mallmann, and R. Schmitt: Phys. Procedia, 83, (2016) 1329.
[38] D. Diego-Vallejo, D. Ashkenasi, A. Lemke, and H. J. Eichler: Spectrochim. Acta B, 87, (2013) 92.
[39] V. P. Bessmeltsev, E. D. Bulushev, and N. V. Goloshevsky: Proc. SPIE, 7996, (2011) 79960C-1.
[40] S. L. Campanelli, G. Casalino, A. D. Ludovico, and C. Bonserio: Int. J. Adv. Manuf. Technol., 66, (2013) 1777.
[41] M. Wiesner, J. Ihlemann, H. H. Müller, E. Lankenau, and G. Hüttmann: Rev. Sci. Instrum., 81, (2010) 33705.
[42] R. Schmitt, G. Mallmann K. Winands, M. Pothen: Photonik International, (2013) 58.
[43] R. Schmitt, G. Mallmann, K. Winands, and M. Pothen: Phys. Procedia, 41, (2013) 887.
[44] B. Neuenschwander, T. Kramer, B. Lauer, and B. Jaeggi: Proc. SPIE, 9350, (2015) 93500U-2.
[45] J. Finger and M. Reininghaus: Opt. Express, 22, (2014) 18790.
[46] C. Hartmann: "Laserabtrag mit zeitlicher Modulation der Energiedeposition", (Apprimus, Aachen, 2014).

(Received: May 17, 2019, Accepted: December 7, 2019)